Comparison of image quality between spectral photon-counting CT and dual-layer CT for the evaluation of lung nodules: a phantom study

Salim A. Si-Mohamed[1,2,3] · Joel Greffier[4] · Jade Miailhes[2] · Sara Boccalini[1,2] · Pierre-Antoine Rodesch[1] · Aurélie Vuillod[5] · Niels van der Werf[6,7] · Djamel Dabli[4] · Damien Racine[8] · David Rotzinger[9] · Fabio Becce[9] · Yoad Yagil[10] · Philippe Coulon[11] · Alain Vlassenbroek[12] · Loic Boussel[1,2] · Jean-Paul Beregi[4] · Philippe Douek[1,2,3]

Abstract

Objectives To evaluate the image quality (IQ) of a spectral photon-counting CT (SPCCT) using filtered back projection (FBP) and hybrid iterative reconstruction (IR) algorithms (iDose^4), in comparison with a dual-layer CT (DLCT) system, and to choose the best image quality according to the IR level for SPCCT.

Methods Two phantoms were scanned using a standard lung protocol (120 kVp, 40 mAs) with SPCCT and DLCT systems. Raw data were reconstructed using FBP and 9 iDose^4 levels (i1/i2/i3/i4/i5/i6/i7/i9/i11) for SPCCT and 7 for DLCT (i1/i2/i3/i4/i5/i6/i7). Noise power spectrum and task-based transfer function (TTF) were computed. Detectability index (d') was computed for detection of 4 mm ground-glass nodule (GGN) and solid nodule. Two chest radiologists performed an IQ evaluation (noise/nodule sharpness/nodule conspicuity/overall IQ) in consensus, and chose the best image for SPCCT.

Results Noise magnitude was −47% ± 2% lower on average with SPCCT than with DLCT for iDose^4 range from i1 to i6. Average NPS spatial frequencies increased for SPCCT in comparison with DLCT. TTF also increased, except for the air insert with FBP, and i1/i2/i3. Higher detectability was found for SPCCT for both GGN and solid nodules. IQ for both types of nodule was rated consistently higher with SPCCT than with DLCT for the same iDose^4 level. For SPCCT and both nodules, the scores for noise and conspicuity improved with increasing iDose^4 level. iDose^4 level 6 provided the best subjective IQ for both types of nodule.

Conclusions Higher IQ for GGN and solid nodules was demonstrated with SPCCT compared with DLCT with better detectability using iDose^4.

Salim Si-Mohamed and Joel Greffier contributed equally to this work.

✉ Salim A. Si-Mohamed
salim.si-mohamed@chu-lyon.fr

1 INSA-Lyon, University of Lyon, University Claude-Bernard Lyon 1, UJM-Saint-Étienne, CNRS, Inserm, CREATIS UMR 5220, U1206, 69100 Villeurbanne, France

2 Radiology Department, Hospices Civils de Lyon, 69500 Lyon, France

3 Department of Cardiovascular and Thoracic Radiology, CHU Cardiologique Louis Pradel, 59 Boulevard Pinel, 69500 Bron, France

4 Department of Medical Imaging, CHU Nimes, Univ Montpellier, Medical Imaging Group, 2415 Nimes, EA, France

5 Medical Physics Department, Hospices Civils de Lyon, 69000 Lyon, France

6 Department of Radiology, University Medical Center Utrecht, Utrecht, The Netherlands

7 Department of Radiology & Nuclear Medicine, Erasmus University Medical Center, Rotterdam, The Netherlands

8 Institute of Radiation Physics, Lausanne University Hospital and University of Lausanne, Rue du Grand-Pré 1, 1007 Lausanne, Switzerland

9 Department of Diagnostic and Interventional Radiology, Lausanne University Hospital and University of Lausanne, Rue du Bugnon 46, 1011 Lausanne, Switzerland

10 Philips Research, Haifa, Israel

11 Philips Research, Suresnes, France

12 CT Clinical Science, 5682 Best, The Netherlands

Key Points

- *Using spectral photon-counting CT compared with dual-layer CT, noise magnitude was reduced with improvements in spatial resolution and detectability of ground-glass nodules and solid lung nodules.*
- *As the iDose^4 level increased, noise magnitude was reduced and detectability of ground-glass and solid lung nodules was better for both CT systems.*
- *For spectral photon-counting CT imaging, two chest radiologists determined iDose^4 level 6 as the best image quality for detecting ground-glass nodules and solid lung nodules.*

Keywords Multidetector computed tomography · Image enhancement · Image reconstruction · Lung · Diagnosis

Abbreviations

DLCT	Dual-layer computed tomography
ESF	Edge spread function
FBP	Filtered back projection
FOV	Field-of-view
GGN	Ground-glass nodule
iDose^4	Intelligent dose
IR	Iterative reconstruction
LSF	Line spread function
NPS	Noise power spectrum
NPWE	Nonprewhitening model observer with eye filter
SPCCT	Spectral photon-counting computed tomography
TTF	Task-based transfer function

Introduction

Lung cancer is the leading cause of death from cancer worldwide, which explains the recent interest in screening strategies in developed countries. Lately, large lung cancer screening cohorts such as the National Lung Screening trial, the NELSON trial, and corollary studies have emphasized the importance of nodule detection to decrease mortality from lung cancer [1, 2].

Conventional computed tomography (CT) equipped with energy-integrating detectors (EIDs) is currently the workhorse for lung imaging. Recently, new detectors with energy-resolving and count of individual incoming photon capabilities, the photon-counting detectors (PCDs), have been implemented in CT systems [3–5]. These detectors, made of much smaller detector elements than standard CT pixel elements, achieve higher spatial resolution than EIDs. One important reason for this is to reduce pulse pile-up effects [6–8]. In addition, they also weight better the low-energy photons that convey the photoelectric effect in soft tissue better, improving the image contrast quality, not to mention the noise efficiency via suppression of electronic noise [9, 10]. Altogether, these properties are key features for potential improved image quality for lung imaging such as recently suggested in vitro and in human imaging [6, 11, 12]. However, these spectral photon-counting CT (SPCCT) systems are still under research and development stage for clinical purposes, with only a few prototypes ready for human imaging [12–15].

Quantitative, objective, and reliable assessment of image quality is essential for assessing the performance of new CT technology or systems such as SPCCT. As with all IR algorithms, iDose^4 has non-linear and non-stationary properties which change the image texture (image smoothing) and make the spatial resolution dependent on dose and contrast [16]. To account for these properties, IR images are now evaluated with new advanced metrics based on clinical tasks. The noise power spectrum (NPS) is used to assess the noise magnitude and frequency content, whereas the task-based transfer function (TTF) is used to evaluate the spatial resolution adapted to a specific clinical task [17–19]. At the end, based on contrast, noise (via NPS), and contrast-dependent spatial resolution (TTF), a mathematical model observer was computed to estimate the radiologist's ability to perform a clinical task such as the detection of lung nodules [18, 20, 21]. This metric is often used in addition to or upstream of a subjective analysis carried out by radiologists from images on patients or anthropomorphic phantom [20, 22]. But knowledge of IQ for SPCCT technology evaluated by these metrics is still missing particularly for lung nodule imaging.

Therefore, the main purpose of the present study was to evaluate the image quality of a clinical SPCCT prototype using filtered back projection (FBP) and a hybrid IR algorithm (iDose^4), in comparison with a standard-of-care dual-layer CT (DLCT) system. In addition, the best image quality for SPCCT was determined according to the IR level for low- and high-contrast lung nodule detection.

Materials and methods

Phantoms

A 20-cm-diameter ACR QA phantom (Gammex) (Fig. 1a) was used to measure physical metrics adapted to IR properties such as the NPS (Fig. 1b) and the TTF (Fig. 1c).
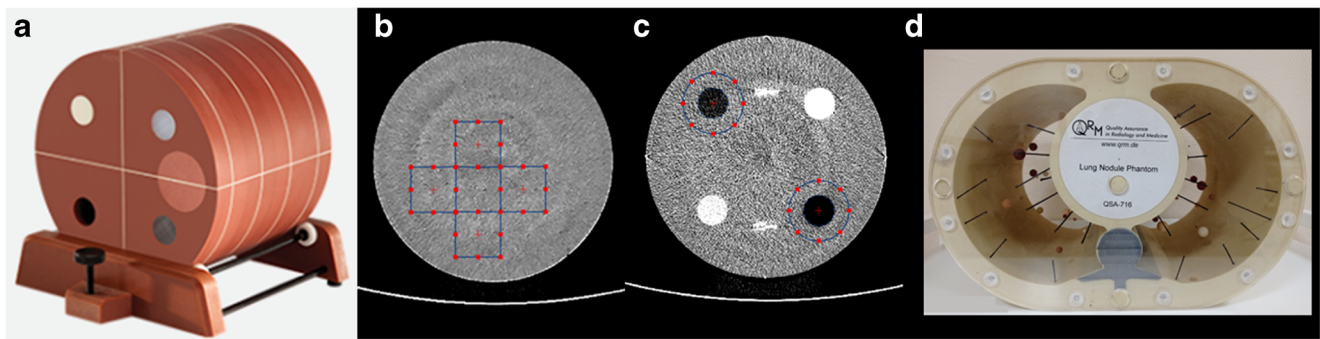
Fig. 1 **a** Image quality phantom used in the study. **b** Regions of interest (ROIs) used for the noise power spectrum (NPS) assessment. **c** ROIs used to compute the task-based transfer function (TTF) with the air and polyethylene inserts

An anthropomorphic lung nodule phantom (QRM-lung nodule phantom) was used to assess subjective image quality for the chest, especially to detect lung nodules (Fig. 1d). Two spherical nodules of 4 mm in diameter were used: one ground-glass nodule (GGN) with a low density of −795 HU at 120 kVp, and one solid nodule with a high density of 20 HU at 120 kVp. To note, we chose nodules with size of 4 mm with respect to the lung CT screening reporting and data system [23]. The difference in attenuation between the background (simulating lung parenchyma) and the nodules was calculated at 200 HU for the GGN and 950 HU for the solid nodule. Two configurations were assessed with and without a tissue-equivalent extension ring, corresponding to a water-equivalent diameter of 21.3 cm (standard patient attenuation) and 27 cm (medium patient attenuation) respectively.

CT systems

The SPCCT system (Philips research and development) is a clinical large field-of-view (FOV) (50 cm in-plane) prototype scanner equipped with energy-sensitive photon-counting detectors (PCDs) with a pixel pitch of 275×275 μm^2 at isocenter, bonded to Philips' proprietary ChromAIX2 application-specific integrated circuit, relying on the direct conversion high band gap semiconductor of cadmium zinc telluride [24]. Each channel offers pulse-height discrimination with five controllable energy thresholds. Further technical details are available in previous study [12]. It supports axial and helical scan modes, tube currents of 10 to 500 mA, tube voltages of 80 to 140 kVp, and rotation times of 0.33 to 1.0 s. Its z-coverage at the isocenter is 17.5 mm. Hybrid IR algorithm iDose^4 was adapted for SPCCT images. The DLCT (IQon, Philips Health Systems) was used as a standard-of-care reference.

Acquisition and reconstruction parameters

Comparable acquisition parameters (rotation time, focal spot, tube current, tube voltage) were used on both CT systems. It should be noted that the beam collimation (clinical beam collimation: 64×0.625 mm) and rotation time (0.27 s/rot) of DLCT were chosen to match the current beam collimation (64×0.275 mm) and rotation time available on SPCCT. The tube current modulation was disabled because it is not yet available on the SPCCT prototype.

For the DLCT, raw data were reconstructed only with FBP and 7 levels of iDose^4 (i1/i2/i3/i4/i5/i6/i7) available with the lung reconstruction kernel YC (Y-Detail) used in our institution for lung imaging (nominal cutoff at 11.5 lp/cm). For the SPCCT, raw data were reconstructed with FBP and 9 iDose^4 levels (i1/i2/i3/i4/i5/i6/i7/i9/i11) out of the 11 levels available with the detailed reconstruction kernel proposed for lung imaging by the constructor (nominal cutoff at 15.8 lp/cm for a 512 matrix size and a 300 mm FOV). For all images and both phantoms, FOV was set at 300 mm and a standard matrix size of 512×512 pixels was used.

The remaining acquisition and reconstruction parameters used for both CT systems are depicted in Table 1.

Task-based image quality assessment

Task-based image quality assessment was carried out using imQuest open-source software package (https://deckard.duhs.duke.edu/~samei/tg233.html). This software assesses the noise texture and magnitude using noise power spectrum (NPS) and spatial resolution using the task-based transfer function (TTF). TTF outcomes for the polyethylene (≈ -95 HU) insert were used for the first lesion and air insert (≈ -1000 HU) for the second. At the end, to estimate the radiologist's ability to detect lesions, a nonprewhitening observer model with an eye filter (NPWE) was used with two simulated tasks: a GGN and a solid nodule of 4 mm in diameter, with the detectability index (d′) used as a figure of merit [17, 18].

The interpretation conditions used to obtain d′ included a 1.5 zoom factor, a viewing distance of 500 mm and a 300-mm FOV to refer to the visualization screen.

The NPS peak was used to quantify changes in magnitude and, to assess noise texture, the average spatial frequency (f_{av}) of the NPS curve and the spatial frequency of the NPS peak (f_{peak}) were measured respectively. To quantify the loss/

Table 1 Acquisition and reconstruction parameters used on the DLCT (dual-layer CT) and the SPCCT (spectral photon-counting CT) systems

	DLCT	SPCCT
Tube voltage (kVp)	120	120
Tube current (mA)	140	140
Rotation time (s/rot)	0.33	0.33
Pitch factor	1.157	1.173
Focal spot (mm × mm)	0.6 × 0.7	0.6 × 0.7
Displayed $CTDI_{vol}$ (mGy)	4.0	3.9
iDose[4] levels	i1/i2/i3/i4/i5/i6/i7	i1/i2/i3/i4/i5/i6/i7/i9/i11
Reconstruction kernel	YC detail	Detailed
Matrix size (number of pixels)	512 × 512	512 × 512
Field-of-view (mm)	300	300
Slice thickness/increment (mm)	0.67/0.34	0.58/0.58

Slice thickness (ST) was set at 0.58 mm contiguous for the SPCCT, i.e., adapted to the reconstructed in-plane pixel size for isotropic voxel size, and at 0.67 mm for the DLCT (minimal slice thickness available). To note, slice increment was set at half of the ST for DLCT images such as performed in clinical practice. Slice increment was similar to ST for SPCCT images enabled by the thinner ST

benefit of spatial resolution, the spatial frequency at which the TTF was reduced by 50% ($TTF_{50\%}$) was measured.

Details of the metrics methodology can be found in the Supplementary Material.

Subjective image quality

All the anthropomorphic phantom images without FBP and iDose[4] levels were read in consensus by 2 chest radiologists (with 10 years (R1) and 6 years (R2) of experience) on a clinical workstation (IntelliSpace Portal, Philips Health Systems) after anonymization. All the images were presented randomly to the readers so they were blinded to the level of iterative reconstruction and the CT system. The images were read only in the transversal planes because of the circularity of the nodules. Readers were blinded to the level of IR and the CT system. They were instructed to assess first the image noise, the nodule conspicuity, and sharpness using a commonly used five-point Likert scale [3; 4] in which 1 = unacceptable, 2 = suboptimal, 3 = acceptable, 4 = above average, and 5 = excellent. A value of less than 3 was considered unsatisfactory for clinical use. They were then asked to assess the overall image quality using a four-point Likert scale as follows: 1 = not evaluable, 2 = interpretable despite moderate artefacts or noise, 3 = fully interpretable with mild artefacts or noise, 4 = no artefacts or noise. Finally, they were asked to choose the best image according to the IR levels for detecting lung nodules with SPCCT imaging.

Radiation dose

CT dose index volumes ($CTDI_{vol}$), determined for a 32-cm-diameter (polymethyl methacrylate) reference phantom, were retrieved from the report available in the CT workstation at the end of all acquisitions.

Results

Task-based image quality assessment

Noise power spectrum

NPS curves obtained for all iDose[4] levels are described in Fig. 2, and values for noise magnitude (square root of the area under the NPS curve), NPS peak, f_{peak}, and f_{av} (noise texture) are given in Table 2. Two peaks on the NPS curves were found for SPCCT, one for spatial frequencies around 0.035 mm^{-1} and the other around 0.836 mm^{-1} (Fig. 2).

For DLCT, NPS peak and noise magnitude decreased with increasing iDose[4] level. Similar results were found for the SPCCT, especially for the peak found at higher spatial frequency (Fig. 2 and Table 2). Between FBP and i6, noise magnitude was reduced by −45% for SPCCT and −49% for DLCT. Similar reductions in noise magnitude between iDose[4] levels were found for both CT systems (for example: −13% between i1 and i2 and −25% i5 and i6 for both CT systems). On average, noise magnitude was −47% ± 2% lower with SPCCT than with DLCT for all iDose[4] levels.

For both CT systems, the values of f_{peak} were similar with increasing iDose[4] levels. Values for f_{peak} were higher with SPCCT than with DLCT (0.836 mm^{-1} vs 0.610 mm^{-1}).

For both CT systems, the values of f_{av} decreased as the iDose[4] level increased. Values for f_{av} were higher with

Table 2 Noise magnitude values (square root of the area under the NPS curve), the magnitude of the peak of the noise power spectrum (NPS peak) curves, spatial frequency (f_{peak}), and average NPS spatial frequency (f_{av}) for all iDose[4] levels on the DLCT (dual-layer CT) and SPCCT (spectral photon-counting CT) systems

iDose[4] Levels	DLCT				SPCCT			
	Noise (HU)	NPS peak (HU^2 mm^2)	f_{peak} (mm^{-1})	f_{av} (mm^{-1})	Noise (HU)	NPS peak (HU^2 mm^2)	f_{peak} (mm^{-1})	f_{av} (mm^{-1})
FBP	170.6	20463	0.610	0.522	96.1	1286/4662	0.035/0.836	0.561
1	152.5	16302	0.610	0.520	83.6	1243/3584	0.035/0.836	0.552
2	142.7	14214	0.610	0.519	77.9	1222/3134	0.035/0.836	0.547
3	132.1	12158	0.610	0.517	72.2	1206/2714	0.035/0.836	0.541
4	120.6	10086	0.610	0.515	64.6	1187/2208	0.035/0.836	0.531
5	107.8	8046	0.610	0.513	57	1164/1754	0.035/0.836	0.518
6	93.4	5994	0.610	0.510	48.6	1149/1311	0.035/0.836	0.497
7	76.4	3969	0.610	0.503	37.5	1117/828	0.035/0.819	0.455
9	-	-	-	-	25.3	1088/410	0.035/0.819	0.369
11	-	-	-	-	18.4	1069/228	0.035/0.819	0.293

SPCCT than with DLCT for FBP and iDose[4] levels ranged from i1 to i5 but were lower from i6 and i7.

Task-based transfer function

For SPCCT, the values of TTF$_{50\%}$ obtained with the polyethylene insert decreased with increasing iDose[4] level (Table 3). Similar values of TTF$_{50\%}$ were found for DLCT as function of iDose[4] levels (ranging from 0.242 to 0.275 mm^{-1}). Values of TTF$_{50\%}$ with SPCCT were higher than those with DLCT for all iDose[4] levels. The differences between TTF values were more marked for the lowest iDose[4] levels.

For the air insert, the values of TTF$_{50\%}$ increased with increasing iDose[4] level (Table 3). Values for TTF$_{50\%}$ were lower with SPCCT than those with DLCT for FBP, i1, i2, and i3 and the opposite afterwards.

Detectability index

The detectability of both detection tasks increased as the iDose4 level increased (Fig. 3). In comparison with DLCT, mean SPCCT d′ were 2.2 ± 0.2 and 1.8 ± 0.1 times higher for the detection of the GGN and solid nodule, respectively, for iDose[4] levels ranging from 1 to 7. For the solid nodule, d′ values of SPCCT were 1.9 and 2.2 higher with i9 and i11 than
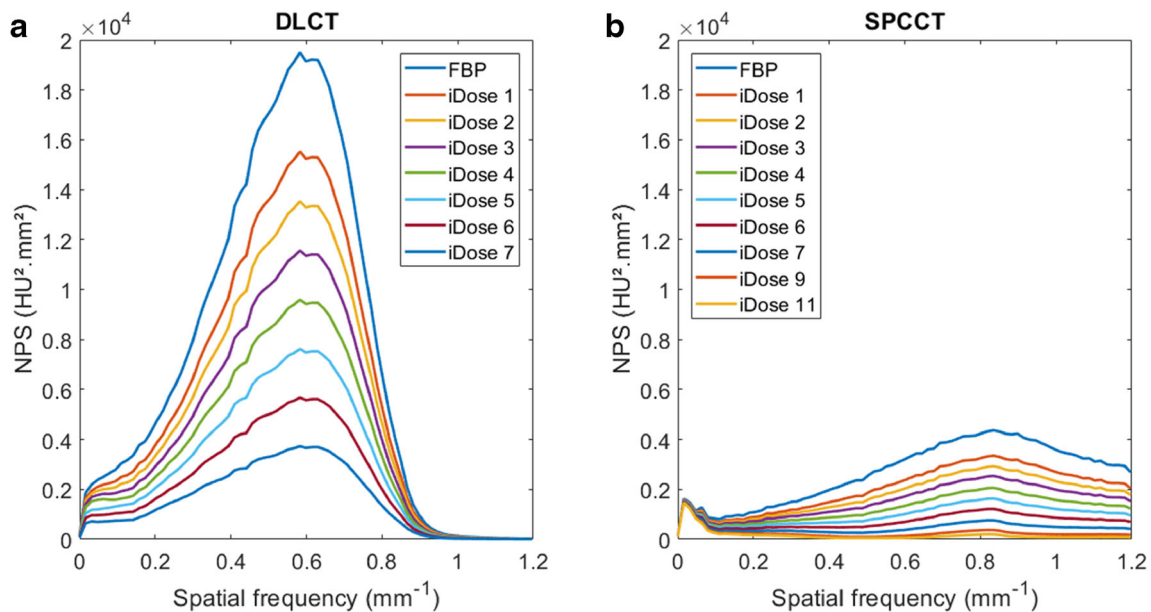

Fig. 2 Noise power spectrum (NPS) curves obtained for all iDose[4] levels and the filtered back projection (FBP) for the DLCT (dual-layer CT) and the SPCCT (spectral photon-counting CT)

Table 3 Value of task-based transfer function at 50% (TTF$_{50\%}$, mm^{-1}) for all iDose^4 levels on the DLCT (dual-layer CT) and SPCCT (spectral photon-counting CT) systems

iDose^4 levels	TTF$_{50\%}$ polyethylene insert (mm^{-1})		TTF$_{50\%}$ air insert (mm^{-1})	
	DLCT	SPCCT	DLCT	SPCCT
0	0.274	0.827	0.644	0.575
1	0.275	0.627	0.657	0.591
2	0.257	0.601	0.657	0.621
3	0.247	0.518	0.662	0.625
4	0.264	0.480	0.663	0.670
5	0.258	0.451	0.671	0.697
6	0.252	0.382	0.687	0.714
7	0.242	0.368	0.694	0.743
9	-	0.319	-	0.779
11	-	0.306	-	0.808

the highest iDose^4 level of the DLCT (i7) and 2.2 and 2.5 for the GGN, respectively.

Subjective image quality

Figure 4 shows the subjective IQ results assessed by the two chest radiologists for both nodule types (Fig. 5). For the same iDose^4 level, scores were consistently higher for SPCCT than for DLCT. Regardless of the CT system, solid nodule quality was rated higher than for GGN. For the SPCCT and both nodule types, the noise and conspicuity scores increased as the iDose^4 level increased. Moreover, the sharpness score increased up to i7 but then decreased for i9 and i11. Similar

results were found for overall image quality. Finally, the radiologists defined i6 as the best image for both types of nodule with SPCCT.

Discussion

In this study, we performed a task-based image quality assessment for lung nodule imaging on an SPCCT scanner developed by Philips Healthcare and equipped with a hybrid IR algorithm (iDose^4). The outcomes demonstrated that SPCCT equipped with PCDs had a lower noise level and a higher spatial resolution compared to a standard-of-care DLCT
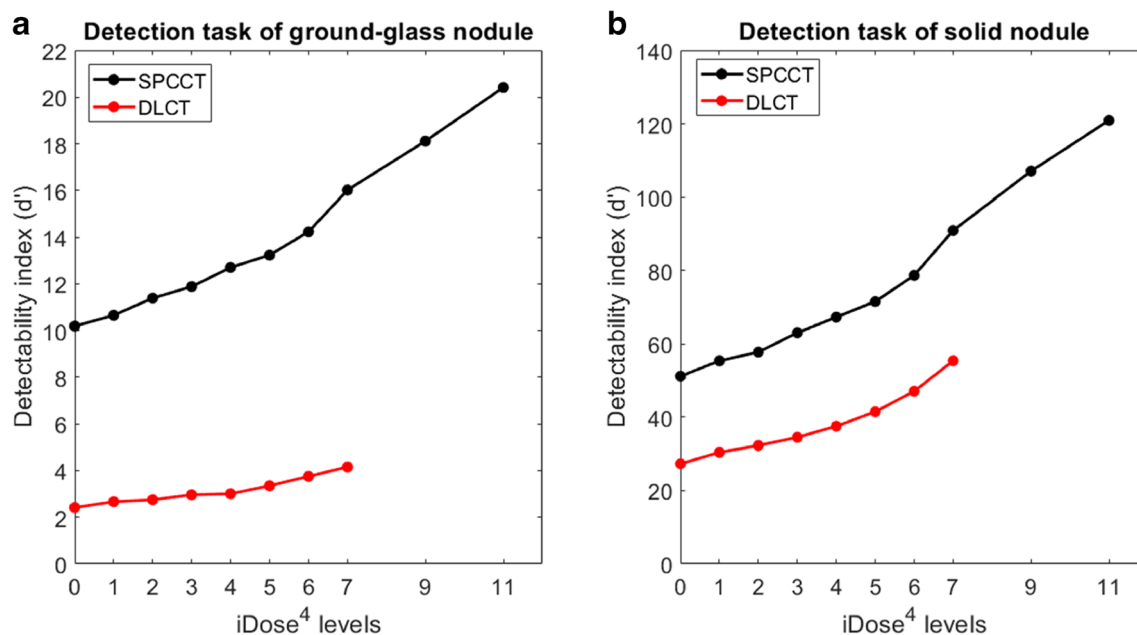

Fig. 3 Detectability index (d′) obtained for dual-layer CT (DLCT) and spectral photon-counting CT (SPCCT) according to iDose^4 levels for the ground-glass nodule (GGN) (**a**) and the solid nodule **b**)
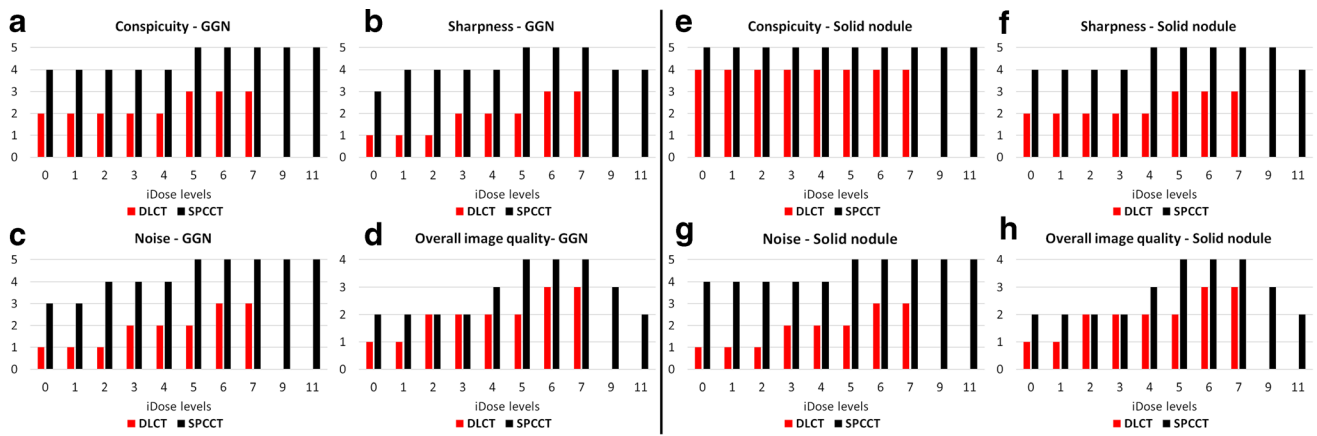
Fig. 4 Lung nodule imaging with spectral photon-counting CT (SPCCT) and dual-layer CT (DLCT). **a**–**d** Ground-glass nodule imaging with SPCCT (**a**, **b**) and DLCT (**c**, **d**) with iDose 0 (left row) and iDose 6 (right row) (empty head arrows). **e**–**h** Solid nodule imaging with SPCCT (**e**, **f**) and DLCT (**g**, **h**) with iDose 0 (left row) and iDose 5 (right row) (empty head arrows). Note that a 2-mm-diameter GGN nearby the replicated thoracic vertebra was hardly visible with DLCT in the anthropomorphic phantom with the extension ring (full head arrows). Rectangles represent close-up view of nodules for better analyzing the image quality

equipped with EIDs from the same manufacturer. Altogether, this resulted in an improvement in detectability on a low-contrast task such as GGN and a high-contrast task such as solid nodule. In addition, the two chest radiologists confirmed a greater image quality of SPCCT and agreed that the best image quality for SPCCT lung nodule imaging was obtained with level 6 of iDose[4].

To the best of our knowledge, this study is the first to evaluate the IQ of an SPCCT system for lung nodule imaging using a task-based model observer assessment. First, the NPS results showed that noise magnitude decreased with increasing iDose[4] levels. These results, common to all IR algorithms, are consistent with previously published studies [17, 20, 21, 25]. The noise reduction per iDose[4] level from i0 to i7 was similar for DLCT and SPCCT. Furthermore, we found that the

noise magnitude calculated for the SPCCT was 47% ± 2% lower in comparison with DLCT. This illustrates the benefits of PCDs for dose efficiency and the suppression of electronic noise compared to EIDs [9, 10]. Differences also existed between the two scanners for the spatial frequency of the NPS peak. Although f_{av} was relatively close for both systems, f_{peak} was higher with SPCCT than with DLCT. This shift towards high frequencies favors the image's fine structures improving image sharpness and image details. We also noted that the use of iDose[4] did not influence the f_{peak} but decreased the f_{av}. The reduction in f_{av} was greater with SPCCT than with DLCT. We also noted the presence of a second low-frequency NPS peak for SPCCT (e.g., 0.035 mm^{-1}), probably related to the presence of a ring-shaped artifact in the center of the image, opening the opportunity to develop specific de-noising algorithms.
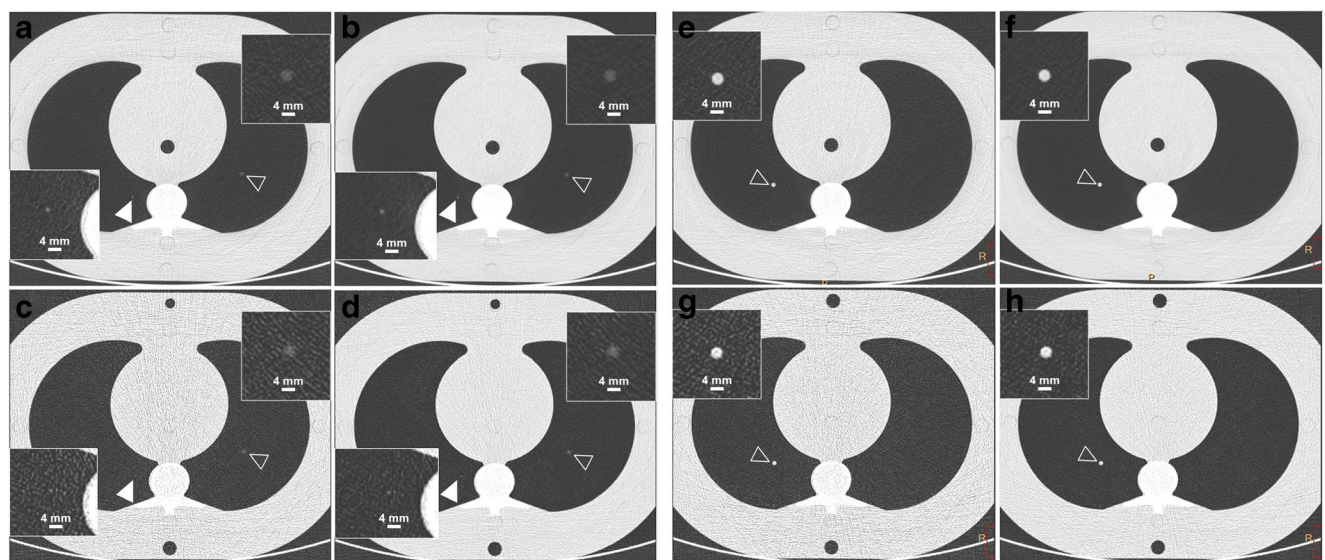

Fig. 5 Subjective analysis according to iDose[4] level: comparison between DLCT (dual-layer CT) and SPCCT (spectral photon-counting CT) imaging. **a**–**d** Ground-glass nodule (GGN) imaging. **e**–**h** Solid nodule imaging

Finally, the different NPS results found with the two scanners can be explained by the use of different parameters such as the reconstruction kernel, slice thickness, collimation (number, type, and size of detectors) and dose level. Nevertheless, the parameters used were chosen for each platform so they convey the best image quality for lung nodule imaging, and do not focus the comparison between the two CT systems on their different detector types. Second, the TTF results for both low- and high-contrast inserts confirmed that the iDose[4] algorithm had non-linear properties, which in particular makes the spatial resolution dependent on contrast. Indeed, for the polyethylene insert (low contrast), the $TTF_{50\%}$ values decreased with increasing iDose[4] level and the opposite was found for the air insert (high contrast). The variations in $TTF_{50\%}$ with iDose[4] level were higher with SPCCT than with DLCT. It is also worth mentioning that the $TTF_{50\%}$ values were higher with SPCCT than with DLCT for the low-contrast insert, especially with the low levels of iDose[4]. Moreover, for the high-contrast insert, similar $TTF_{50\%}$ values were found for both CT systems. Finally, these results demonstrated that SPCCT had a higher spatial resolution than DLCT improving the nodules' border. Indeed, the d′ results showed that the highest detectability was found with higher iDose[4] levels. This finding is in agreement with previously published results for iDose[4] and other IR algorithms [20, 26]. In addition, we found that the detectability of both low- and high-contrast nodules was higher with SPCCT than with DLCT, whatever the iDose[4] level. These results were directly related to the NPS and TTF outcomes. Altogether with a lower noise magnitude, a higher NPS spatial frequency and higher or similar TTF values than with DLCT, the d′ values were higher with SPCCT.

The subjective image quality assessment of GGN and solid nodule in an anthropomorphic phantom confirmed the NPS and TTF outcomes found in the task-based image quality assessment. Both readers confirmed that image noise decreased with increasing iDose[4] levels and that noise was subjectively lower with SPCCT than with DLCT. Similar results were found for GGN conspicuity. For the solid nodule, the highest score was graded irrespective of the iDose[4] level for SPCCT and the sharpness score was rated as 4 from i0 to i3, 5 from i4 to i9, and then decreased afterwards. The lowest sharpness score was found for the GGN, with a score at 3 for i0, 4 from i1 to i4, 5 from i5 to i7, and decreased afterwards. Therefore, the overall image quality was higher with SPCCT than DLCT for both nodules and the highest scores were found from i5 to i7. Finally, the radiologists agreed that the best image quality for both nodules was obtained with level i6. According to these findings, it is worth noting that a 2-mm-diameter GGN in the phantom surrounded by an extension ring was only seen with SPCCT, confirming the significant gain in GGN detectability with SPCCT. In addition, this result differs from that found with the d′ values of both nodules. Indeed, modifications in image texture (especially image smoothness) with the highest iDose[4] levels decreased the nodule sharpness score and, therefore, overall image quality. This result confirms that a subjective assessment of image quality is necessary to take into account the radiologist's feeling for this type of image, in addition to task-based image quality assessment [16]. However, the results found in this study should be toned down because we used phantoms that did not accurately represent the patient morphology, the lung tissue attenuation, and the different structural changes in the parenchyma. Indeed, many studies have shown that IR algorithms change the image texture (especially for high IR levels) and the tissue sharpness and border, which can impede the radiologists in its interpretation. Further patient studies on lung CT images could be performed to validate and confirm these results found on phantoms.

Our study has certain limitations. First, the image quality had been evaluated only on circular nodules and therefore the IQ may differ on spiculated lesions. Second, the absence of volumetric assessment may limit the ability to transfer our findings to spiculated lesions. Third, we did not evaluate the impact of iDose[4] depending on the radiation dose: investigations under low- and ultra-low-dose conditions need to be performed. Fourth, we did not investigate the impact of higher matrix size or small slice thickness which may offer higher spatial resolution performances with SPCCT. Finally, the different results found for the two scanners may be explained by the use of different parameters such as the reconstruction kernel, slice thickness, and collimation (number, type, and size of detectors) despite our attempts to make these parameters comparable.

Conclusion

A clinical SPCCT prototype outperformed a standard-of-care DLCT system in the evaluation of GGN and solid nodules, with improvements in their detectability using hybrid IR algorithms, suggesting a great interest for the use of SPCCT in lung cancer imaging.

Declarations

Guarantor The scientific guarantor of this publication is Pr. Philippe DOUEK.

References

1. de Koning HJ, van der Aalst CM, de Jong PA et al (2020) Reduced lung-cancer mortality with volume CT screening in a randomized trial. N Engl J Med 382:503–513. https://doi.org/10.1056/NEJMoa1911793

2. National Lung Screening Trial Research Team, Aberle DR, Adams AM et al (2011) Reduced lung-cancer mortality with low-dose computed tomographic screening. N Engl J Med 365:395–409. https://doi.org/10.1056/NEJMoa1102873

3. Si-Mohamed S, Boussel L, Douek P (2020) Clinical applications of spectral photon-counting CT. In: Spectral, photon counting computed tomography: technology and applications, CRC Press. pp 97–116

4. Si-Mohamed S, Bar-Ness D, Sigovan M et al (2017) Review of an initial experience with an experimental spectral photon-counting computed tomography system. Nucl Inst Methods Phys Res B 873:27–35. https://doi.org/10.1016/j.nima.2017.04.014

5. Taguchi K, Iwanczyk JS (2013) Vision 20/20: Single photon counting x-ray detectors in medical imaging. Med Phys 40: 100901. https://doi.org/10.1118/1.4820371

6. Kopp FK, Daerr H, Si-Mohamed S et al (2018) Evaluation of a preclinical photon-counting CT prototype for pulmonary imaging. Sci Rep 8:17386. https://doi.org/10.1038/s41598-018-35888-1

7. Sigovan M, Si-Mohamed S, Bar-Ness D et al (2019) Feasibility of improving vascular imaging in the presence of metallic stents using spectral photon counting CT and K-edge imaging. Sci Rep 9: 19850. https://doi.org/10.1038/s41598-019-56427-6

8. Si-Mohamed S, Thivolet A, Bonnot P-E et al (2018) Improved peritoneal cavity and abdominal organ imaging using a biphasic contrast agent protocol and spectral photon counting computed tomography K-edge imaging. Invest Radiol 53:629–639. https://doi.org/10.1097/RLI.0000000000000483

9. Blevis I (2020) X-Ray detectors for spectral photon-counting CT. In: Spectral, photon counting computed tomography: technology and applications, CRC Press. pp 179–191

10. Hsieh (2020) Design considerations for photon-counting detectors: connecting detectors characteristics to system performances. In: Spectral, photon counting computed tomography: technology and applications, CRC Press. pp 326–341

11. Bartlett DJ, Koo CW, Bartholmai BJ et al (2019) High-resolution chest computed tomography imaging of the lungs: impact of 1024 matrix reconstruction and photon-counting detector computed tomography. Invest Radiol 54:129–137. https://doi.org/10.1097/RLI.0000000000000524

12. Si-Mohamed S, Boccalini S, Rodesch P-A et al (2021) Feasibility of lung imaging with a large field-of-view spectral photon-counting CT system. Diagn Interv Imaging. https://doi.org/10.1016/j.diii.2021.01.001

13. da Silva J, Grönberg F, Cederström B et al (2019) Resolution characterization of a silicon-based, photon-counting computed tomography prototype capable of patient scanning. J Med Imaging (Bellingham) 6, 043502. https://doi.org/10.1117/1.JMI.6.4.043502

14. Boccalini S, Si-Mohamed S, Dessouky R, Sigovan M, Boussel L, Douek P. (2021) Feasibility of human vascular imaging of the neck with a large field-of-view spectral photon-counting CT system. Diagn Interv Imaging. https://doi.org/10.1016/j.diii.2020.12.004

15. Ferda J, Vendiš T, Flohr T et al (2021) Computed tomography with a full FOV photon-counting detector in a clinical setting, the first experience. Eur J Radiol 137:109614. https://doi.org/10.1016/j.ejrad.2021.109614

16. Greffier J, Fernandez A, Macri F, Freitag C, Metge L, Beregi JP (2013) Which dose for what image? Iterative reconstruction for CT scan. Diagn Interv Imaging 94:1117–1121. https://doi.org/10.1016/j.diii.2013.03.008

17. Greffier J, Frandon J, Larbi A, Beregi JP, Pereira F (2019) CT iterative reconstruction algorithms: a task-based image quality assessmen. Eur Radiol. https://doi.org/10.1007/s00330-019-06359-6

18. Samei E, Richard S (2015) Assessment of the dose reduction potential of a model-based iterative reconstruction algorithm using a task-based performance metrology. Med Phys 42:314–323. https://doi.org/10.1118/1.4903899

19. Verdun FR, Racine D, Ott JG et al (2015) Image quality in CT: from physical measurements to model observers. Phys Med 31: 823–843. https://doi.org/10.1016/j.ejmp.2015.08.007

20. Greffier J, Boccalini S, Beregi JP et al (2020) CT dose optimization for the detection of pulmonary arteriovenous malformation (PAVM): a phantom study. Diagn Interv Imaging. https://doi.org/10.1016/j.diii.2019.12.009

21. Rotzinger DC, Racine D, Beigelman-Aubry C et al (2018) Task-based model observer assessment of a partial model-based iterative reconstruction algorithm in thoracic oncologic multidetector CT. Sci Rep:8. https://doi.org/10.1038/s41598-018-36045-4

22. Greffier J, Frandon J, Pereira F et al (2020) Optimization of radiation dose for CT detection of lytic and sclerotic bone lesions: a phantom study. Eur Radiol 30:1075–1078. https://doi.org/10.1007/s00330-019-06425-z

23. American College of Radiology (2015) Lung CT screening reporting and data system lung-RADS). https://www.acr.org/Clinical-Resources/Reporting-and-Data-Systems/Lung-Rads.

24. Steadman R, Herrmann C, Livne A (2017) ChromAIX2: a large area, high count-rate energy-resolving photon counting ASIC for a spectral CT prototype. Nucl Inst Methods Phys Res B 862:18–24. https://doi.org/10.1016/j.nima.2017.05.010

25. Greffier J, Larbi A, Frandon J et al (2019) Comparison of noise-magnitude and noise-texture across two generations of iterative reconstruction algorithms from three manufacturers. Diagn Interv Imaging 100:401–410. https://doi.org/10.1016/j.diii.2019.04.006

26. Greffier J, Si-Mohamed S, Dabli D et al (2021) Performance of four dual-energy CT platforms for abdominal imaging: a task-based image quality assessment based on phantom data. Eur Radiol. https://doi.org/10.1007/s00330-020-07671-2